Analysis of Retrieval Accuracy and Spatial–Temporal Variation of Chlorophyll-A Concentration in Bohai Sea Based on GOCI

Jing-wen Hu, Xiao-yan Liu, Qi-xiang Wang, Xin Li, Wen-long Dong, Wei-qi Lin, Jun-yue Zhang, Ming-yu Li, and Zhi-hong Wu

***Abstract*—Bohai Sea is China's inland sea, its complex marine and atmospheric optical properties pose a challenge to the application of satellite data to retrieve chlorophyll-a (CHLA) concentration with high accuracy. The high accuracy retrieval results of CHLA require simultaneous consideration of the adaptability of atmospheric correction algorithms and CHLA retrieval models. In this study, four atmospheric correction methods [the standard atmospheric correction algorithms of GDPS1.4.1 and GDPS2.0, the standard near-infrared atmospheric correction algorithm of NASA (Seadas_Default), and management unit of the North Sea mathematical models (Seadas_MUMM)] and four CHLA retrieval models (OC2, YOC, OC3G, and OC2M-HI) were selected in the process of applying geostationary ocean color imager (GOCI) data to retrieve CHLA in Bohai Sea. Based on the in situ data, the adaptability of their pairwise combinations in retrieval of CHLA in Bohai Sea was evaluated. The results indicate that the OC2 and OC3G models significantly overestimated the CHLA. The combination of the Seadas_Default atmospheric correction algorithm with the YOC CHLA retrieval model, or the combination of the Seadas_MUMM atmospheric correction algorithm with the YOC CHLA retrieval model, is more suitable for the retrieval of CHLA using GOCI data in Bohai Sea. In addition, this study shows that the CHLA obtained based on the data from eight-scene GOCI data were different to the data obtained based on single-scene GOCI data (approximating traditional polar-orbiting satellite sensor data) in daily, monthly, and yearly average results. The monthly mean difference between the two is the most significant, ranging from -0.66 to 1.49 μg/l.**

Manuscript received 31 January 2024; revised 20 April 2024 and 23 May 2024; accepted 5 June 2024. Date of publication 14 June 2024; date of current version 5 August 2024. This work was supported in part by the Open Foundation of Weifang Key Laboratory of Satellite Remote Sensing Intelligent Interpretation Technology under Grant SYS202303, in part by the National Key Research and Development Program of China under Grant 2019YFC1408003, and in part by the Natural Science Foundation of Shandong Province under Grant ZR2023QD023, Grant ZR2022QD061, and Grant ZR2021QD135. *(Corresponding author: Zhi-hong Wu.)*

Jing-wen Hu is with the Weifang Key Laboratory of Satellite Remote Sensing Intelligent Interpretation Technology, Weifang 261021, China, and also with the Shandong Marine Forecast and Hazard Mitigation Service, Qingdao 266000, China (e-mail: hujingwen@shandong.cn).

Xiao-yan Liu, Wei-qi Lin, Jun-yue Zhang, and Ming-yu Li are with the Institute of Oceanographic Instrumentation, Qilu University of Technology (Shandong Academy of Sciences), Qingdao 266000, China (e-mail: liuxiaoyan@qlu.edu.cn; linwq0908@163.com; junyuezhang2024@163.com; limingy0112@163.com).

Qi-xiang Wang, Wen-long Dong, and Zhi-hong Wu are with the Shandong Marine Forecast and Hazard Mitigation Service, Qingdao 266000, China (e-mail: wqxbx@163.com; dongwenlong529@163.com; wuzhihong@aliyun.com).

Xin Li is with the Weifang Marine Development Research Institute, Weifang 261021, China (e-mail: maliao0919@163.com).

Digital Object Identifier 10.1109/JSTARS.2024.3414588

***Index Terms*—Atmospheric correction, Bohai Sea, chlorophyll-a (CHLA), geostationary ocean color imager (GOCI).**

I. Introduction

BOHAI Sea (see Fig. 1) is a semienclosed inland sea surrounded by land on three sides, and it is the only one of its kind in China. It has numerous rivers along its coast, and it serves as a convergence point for three of China's seven major water systems: the Yellow River, Hai River, and Liao River systems. With the development and construction of the 13 coastal cities around the Bohai Sea, the amount of land-based pollutant emissions has been increasing year by year, greatly impacting the marine ecological environment quality of the Bohai Sea [1], [2], [3], [4]. In recent years, in order to promote the sustainable development of the Bohai Sea and the rational utilization of marine resources, relevant government authorities in China have introduced a series of policies and measures. Therefore, it is of great significance to conduct research on the spatial and temporal variations of key ecological factors and water quality parameters in the Bohai Sea to sustainably monitor and evaluate the ecological environment regulatory work, including monitoring the concentration of chlorophyll-a (CHLA) in the Bohai Sea.

CHLA concentration of the water is a key indicator of marine phytoplankton biomass, and one of the basic parameters for measuring marine net primary production and eutrophication. Studying its spatial–temporal changes provides necessary reference for in-depth analysis of global hot issues, such as changes in marine ecosystems, global carbon cycles, and climate change [5], [6]. Traditional observations of CHLA concentrations are often conducted through marine buoys or aerial surveys, which are not only time-consuming and laborious but also difficult to conduct large-scale investigations [7], [8]. Remote sensing technology, with its fast imaging speed, multiple spectral bands, wide imaging range, long time series, and low economic cost, has rapidly become an important means of obtaining ecological information, such as CHLA concentrations [9]. In recent years, mainstream remote sensing inversion algorithms for CHLA concentrations are mostly based on empirical algorithms and semianalytical algorithms [10], [11], [12], [13], [14], [15], [16], [17], [18], [19], [20], [21], [22], [23], and some researchers have tried to estimate CHLA concentrations using machine learning

methods, such as neural networks [24], [25]. But overall, the primary reliance for the retrieval of CHLA concentration using satellite data is the remote sensing reflectance (R_{rs}) data of the water, for example, the OC2 algorithm [26] and OC2M-HI algorithm [27] are both based on the R_{rs} data at 490 and 555 nm wavelengths, YOC algorithm [28] is based on the R_{rs} data at 412, 443, 490, and 555 nm wavelengths, and OC3G algorithm [29] is based on the R_{rs} data at 443, 490, and 555 nm wavelengths. High-quality marine remote sensing research requires precise R_{rs} data as a basis [30], [31]. Obtaining R_{rs} data of the water from satellite sensor data requires atmospheric correction. Effective atmospheric correction algorithms proposed by international scholars for near-shore case II turbid water include dark pixel method [32], [33], bright pixel method [34], [35], neural network method [36], [37], [38], spectral matching optimization method [39], [40], [41], etc. Research shows that there are significant differences between R_{rs} data obtained from the same satellite data when using different atmospheric correction algorithms in the same sea area [42], and differences in ecological parameter retrieval algorithms for the same sea area can also cause huge differences in retrieval results [16]. But there is still a lack of literature on wide-ranging joint evaluation of the accuracy of specific sea area ecological parameter retrieval by unifying atmospheric correction algorithms and ecological parameter retrieval algorithms. Currently, the number of available atmospheric correction algorithms and CHLA concentration retrieval algorithms is numerous, and different combination pairs may cause differences in retrieval accuracy. Therefore, evaluating the reliability of various CHLA concentration retrieval algorithms under different atmospheric correction algorithms has important application value. In addition, most of the spatio–temporal change analyses of CHLA concentration by domestic and foreign scholars are based on polar-orbiting satellite data (such as MODIS and SeaWiFS) [43], [44]. However, the studies about marine ecological elements (such as transparency, sea surface salinity, and CHLA) based on geostationary ocean color imager (GOCI) show that the hourly variation difference cannot be ignored [45], [46], [47], [48]. Therefore, it is significant to compare the spatio–temporal changes of CHLA concentration in Bohai Sea based on the multifrequency observations of GOCI with the results based on single observation data.

GOCI, the primary sensor mounted on the geostationary satellite COMS, provides up to eight daily observations (GOCI II provides ten daily observations). In comparison with polar-orbiting satellites, GOCI significantly enhances the temporal resolution and spatial coverage of remote sensing data. This improvement enables the monitoring of short-term changes in coastal water quality and large algae. It is also particularly crucial for studying the long-term variations in bio-optical parameters [49], [50]. GOCI data processing system (GDPS) is a specialized software designed for the analysis and processing of GOCI sensor data, specifically allowing for atmospheric correction. Korea Ocean Satellite Center (KOSC) has, to date, offered six versions of GDPS (GDPS 1.1, GDPS 1.2, GDPS 1.3, GDPS 1.4, GDPS 1.4.1, and GDPS 2.0) to users worldwide free of charge. SeaDAS is a dedicated software for processing water color remote sensing data. It performs atmospheric correction on satellite data and uses NASA's standard atmospheric correction algorithm as its default (SeaDAS_Default). In addition, SeaDAS provides the management unit of the North Sea mathematical model (MUMM) atmospheric correction algorithm (SeaDAS_MUMM) for user.

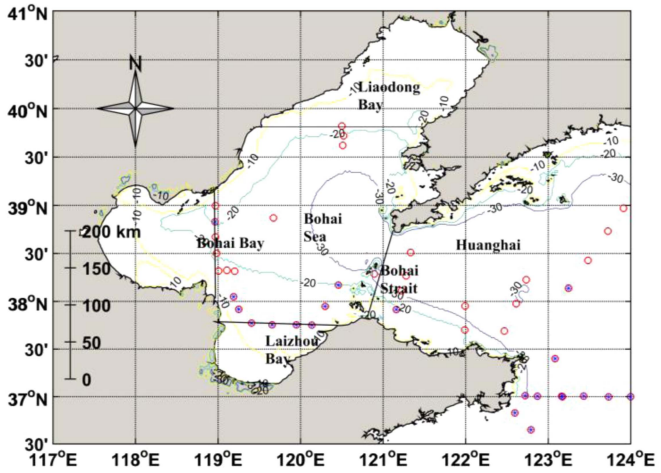

Fig. 1. Location map of Bohai Sea. The red dots represent the locations of the measurement stations, and the contour lines represent the water depth. The blue dots represent that the stations can be paired with the data retrieved from GOCI under clear skies.

In this study, in the process of retrieval of CHLA concentration in Bohai Sea using GOCI data, four operational atmospheric correction algorithms and four CHLA concentration retrieval algorithms were used for pairwise combination. Then, 16 groups of retrieved results were compared with the in situ CHLA concentration data, respectively, to select the most suitable combination of atmospheric correction and CHLA concentration retrieval algorithm for the Bohai Sea. The selected algorithm combination was applied to retrieve CHLA concentration using GOCI data from April 2011 to March 2021, and the temporal and spatial changes of CHLA concentration in Bohai Sea in the ten years were analyzed.

II. Data

A. In Situ Data

The field sampling and laboratory measurement of CHLA concentration were conducted in the Bohai Sea on 30 April, 2014, 3 May, 2014, 12 May, 2014, 10 September, 2015, 16 May, 2017, and 9–12 March, 2018. A total of 42 measured station data were obtained. The red dots in Fig. 1 represent the locations of the measurement stations. In total, 21 measured CHLA concentration of these stations (blue dots in Fig. 1) can be paired with the data retrieved from GOCI under clear skies. The measurement method for CHLA concentration was used spectrophotometry. The specific procedure involved obtaining 2–5 L of seawater sample, adding 3 ml of magnesium carbonate suspension, mixing thoroughly, and filtering through a 0.45-μm cellulose acetate membrane filter. The filtered membrane was placed in a centrifuge tube, and 10 ml of acetone solution was added. The mixture was shaken and left to stand in a refrigerator

for 14–24 h to extract the CHLA concentration. The supernatant of the extraction (v ml) was transferred to a measurement cell, and acetone solution was used as a reference. The absorbance values were measured at wavelengths of 750, 664, 647, and 630 nm using a spectrophotometer. The measurement at 750 nm was used to correct for the turbidity of the extraction solution. If the absorbance value at a 1-cm measurement cell exceeded 0.005, the extraction solution needed to be recentrifuged. The absorbance values at 664, 647, and 630 nm were subtracted from the absorbance value at 750 nm to obtain the corrected absorbance values (E664, E647, E630). The concentration of CHLA was then calculated using the following equation:

$$\begin{aligned}\mathrm{CHLA} &= (11.85 \times \mathrm{E664} - 1.54 \times \mathrm{E647} - 0.08 \times \mathrm{E630}) \\ &\quad \times \mathrm{v}/(\mathrm{V} \times \mathrm{L}) \end{aligned} \tag{1}$$

The unit of CHLA is μg/l, where v represents the volume of the sample extraction (ml), V denotes the actual volume of seawater sample used (l), and L stands for the path length of the measurement cell (cm).

B. GOCI Data

The swath width of GOCI imagery is 2500 × 2500 km, covering the Bohai Sea, Yellow Sea, and parts of the East China Sea. It has a spatial resolution of 500 m and a spectral range of 0.412–0.865 μm, including six visible light bands and two near-infrared bands. It acquires eight-scene observation data per day, from Beijing local time 8 A.M. to 15 P.M., with one scene per hour. The L1B data used in this study were provided by the KOSC for the period from 1 April, 2011 to 31 March, 2021.

C. GMI Data

The GMI microwave radiometer was carried on the global precipitation measurement satellite and was successfully launched on 27 February, 2014. In this study, we selected the global monthly average data of GMI from January 2015 to January 2020, which can provide data values, such as sea surface temperature, rain rate, and wind speed. The download address is available online.[1]

III. Algorithm

A. Atmospheric Correction Algorithm

The target of atmospheric correction is to get surface water reflectance, $\rho_{\mathrm{w}}(\lambda)$, extracted from the top of atmosphere [$\rho(\lambda)$] measured by satellite. Ignoring the surface-reflectance from Sun-glint and whitecaps, $\rho(\lambda)$ can be described as follows [51]:

$$\rho(\lambda) = \rho_{\mathrm{r}}(\lambda) + \rho_{\mathrm{a}}(\lambda) + t\rho_{\mathrm{w}}(\lambda) \tag{2}$$

where ρ_{r} is the Rayleigh multiple-scattering reflectance in the absence of aerosols, and ρ_{a} is the aerosol multiple-scattering reflectance in the presence of air molecules. t is the diffuse transmittance of the atmosphere from the Sun to the sea surface and from the sea surface to the sensor.

[1][Online]. Available: https://www.remss.com/missions/gmi/

TABLE I
Relations of Each Spectral Band

λ1 (nm)	555	555	555	745	745	745	865
λ2 (nm)	412	430	490	555	660	680	745
D	4	4	4	4	3	3	2

$\rho_{\mathrm{r}}(\lambda_0)$ can be obtained based on precalculations through radiative transfer simulations. Then, the $\rho_{\mathrm{a}}(\lambda_0)$ of the corresponding NIR bands and β in (3) can be calculated by using the measured data $\rho(\lambda_0)$ through (2) and (3) by assuming the value or ratio relationship of the $\rho_w(\lambda_0)$ of the two NIR bands. Then, the $\rho_{\mathrm{a}}(\lambda)$ at any wavelength can be calculated by the following equation, and finally, the $\rho_{\mathrm{w}}(\lambda)$ at any wavelength can be calculated by (2):

$$\rho_{\mathrm{a}}(\lambda_{\mathrm{i}}) = (\lambda_{\mathrm{i}}/\lambda_{\mathrm{j}})^{-\beta}\rho_{\mathrm{a}}(\lambda_{\mathrm{j}}). \tag{3}$$

GDPS is the official software provided by KOSC for processing GOCI data. GDPS1.1 and GDPS1.2 used the empirical relation between the red band and NIR water-leaving reflectance to calculate the NIR reflectance ρ_{w} (4) due to the lack of NIR band information in GOCI [52]

$$\begin{aligned}\rho_{\mathrm{w}}(745) &= \sum_{n=1}^{4} j_n \rho_w^n(660) \\ \rho_{\mathrm{w}}(865) &= 1.936 \times \rho_{\mathrm{w}}(745). \end{aligned} \tag{4}$$

GDPS1.3 modified the above equations [53]

$$\begin{aligned}\rho_{\mathrm{w}}(745) &= \sum_{n=1}^{6} j_n \rho_w^n(660) \\ \rho_{\mathrm{w}}(865) &= \sum_{\mathrm{n}=1}^{2} \mathrm{k_n}\rho_{\mathrm{w}}(745). \end{aligned} \tag{5}$$

The GDPS1.4∗ mainly updates the software modularization based on the GDPS1.3, without changing the atmospheric correction algorithm [53]. The atmospheric correction of GDPS2.0 takes advantage of the spectral relationship between the reflectance of multiple scattering of aerosols at different wavelengths, called the spectral relationships in the aerosol multiple-scattering reflectance (SRAMS) between different wavelengths to calculate the reflectance contribution of near-infrared multiple scattering directly. Then, SRAMS spectra were used to estimate the reflection contribution of the aerosol model in the near infrared band to the visible band [54]. The spectral relationship between the reflection spectra of multiple scattering aerosols and different wavelengths is established by polynomial function (6), and the relations of the spectral segment are summarized in Table I

$$\rho_w(\lambda_2) = \sum_{n=1}^{D} c_n \rho_w{}^{\mathrm{n}}(\lambda_1) \tag{6}$$

Where D represents the calculation order.

Based on this, we used the atmospheric correction algorithm of GDPS1.4.1 and GDPS2.0 to process the GOCI L1B data and got the corrected R_{rs} data.

In addition, two atmospheric correction algorithms of SeaDAS 8.2 (Seadas_Default and Seadas_MUMM) were selected to process the atmospheric correction on GOCI data, and the corrected R_{rs} data were obtained. The NASA standard atmospheric correction algorithm (i.e., Seadas_Default in this study) was originally developed by Gordon and Wang [55] in 1994, and was extended its application to case II waters by Stumpf et al. [56] in 2003, and further was revised by the authors in [57] and [58]. NASA uses this algorithm as the default atmospheric correction algorithm of SeaDAS to process the ocean color remote sensing data and provides L2 products for users. The MUMM atmospheric correction algorithm was proposed by Ruddick [59] in 2000,which assumed that the aerosol multiple scattering reflectance ratio of the two near-infrared bands of each pixel is a fixed value and the ratio between reflectance and atmospheric transmission at the two near-infrared bands is constant.

B. CHLA Retrieval Algorithm

Many retrieval models of CHLA concentration have been proposed and applied in the world currently. This article selects four representative CHLA concentration retrieval models, OC2, YOC, OC3G, and OC2M-HI, and matches them with the four atmospheric correction algorithms selected above to analyze their reliability in the sea area studied in this article.

OC2 is a cubic polynomial algorithm proposed by Hooker et al. [26] based on the ratio of R_{rs} in the 490- and 555-nm bands. Its algorithm expression is

$$\mathrm{CHLA} = e_0 + 10^{e_1+e_2\times R+e_3\times R^2+e_4\times R^3} \tag{7}$$

$$R = \log_{10}\left(\frac{\mathrm{R_{rs}}(490)}{\mathrm{R_{rs}}(555)}\right) \tag{8}$$

where $e_0 = -0.0929$, $e_1 = 0.2974$, $e_2 = -2.2429$, $e_3 = 0.8358$, and $e_4 = -0.0077$.

YOC was obtained by Siswanto et al. [28] after optimizing the parameters of the CHLA concentration retrieval algorithm proposed by Tassan et al. [60] based on measured data. It is a quadratic polynomial algorithm based on the R_{rs} ratio in the 412-, 443-, 490-, and 555-nm bands. Its algorithm expression is

$$\mathrm{CHLA} = 10^{c_1-c_2\times\log_{10}^{(R)}-c_3\times\log_{10}^2(R)} \tag{9}$$

$$R = \frac{R_{rs}(443)}{R_{rs}(555)}\left(\frac{R_{rs}(412)}{R_{rs}(490)}\right)^{C_4} \tag{10}$$

where $c_1 = 0.342$, $c_2 = 2.511$, $c_3 = 0.277$, and $c_4 = -1.012$.

OC3G is a fourth-order polynomial algorithm [29] based on the OC4 algorithm [61], which uses the maximum ratio of R_{rs} (443)/R_{rs} (555) to R_{rs} (490)/R_{rs} (555) to establish a fourth-order polynomial algorithm. Its algorithm expression is

$$\mathrm{CHLA} = 10^{f_0+f_1\times R+f_2\times R^2+f_3\times R^3+f_4\times R^4} \tag{11}$$

$$R = \log_{10}\frac{\max\left[Rrs(443),\ Rrs(490)\right]}{Rrs(555)} \tag{12}$$

where $f_0 = 0.366$, $f_1 = -3.067$, $f_2 = 1.93$, $f_3 = 0.649$, and $f_4 = -1.532$.

The OC2M-HI algorithm [27] developed by the members of NASA is also a widely used CHLA concentration retrieval algorithm, which is a fourth-order polynomial algorithm based on the ratio of R_{rs} in the 490- and 555-nm bands. Its algorithm expression is

$$\mathrm{CHLA} = 10^{a_1-a_2\times R+a_3\times R^2-a_4\times R^3-a_5\times R^4} \tag{13}$$

$$\mathrm{R} = \log_{10}\left(\frac{R_{rs}(469)}{R_{rs}(555)}\right) \tag{14}$$

where $a_1 = 0.1464$, $a_2 = 1.7953$, $a_3 = 0.9718$, $a_4 = 0.8319$, and $a_5 = 0.8073$. Due to GOCI was not set the band of 469 nm, this article uses interpolation method to obtain R_{rs} data in the 469-nm band.

C. Accuracy Evaluation

The correlation coefficient r, root-mean-square error RMSE, and the averaged unbiased percentage difference ε were calculated to assess the accuracy of validation, and goodness-of-fit as follows:

$$\mathrm{r} = \frac{\sum_{\mathrm{i}=1}^{n}\left(X^i{}_{\mathrm{chla-est}}-\overline{X}\right)\left(Y^i{}_{\mathrm{chla-mea}}-\overline{Y}\right)}{\sqrt{\sum_{\mathrm{i}=1}^{n}\left(X^i{}_{\mathrm{chla-est}}-\overline{X}\right)^2\left(Y^i{}_{\mathrm{chla-mea}}-\overline{Y}\right)^2}} \tag{15}$$

$$\mathrm{RMSE} = \sqrt{\frac{1}{\mathrm{n}}\cdot\sum_{\mathrm{i}=1}^{n}\left(X^i{}_{\mathrm{chla-est}}-Y^i{}_{\mathrm{chla-mea}}\right)^2} \tag{16}$$

$$\varepsilon = \frac{1}{\mathrm{n}}\cdot\sum_{\mathrm{i}=1}^{n}\left[X^i{}_{\mathrm{chla-est}}-Y^i{}_{\mathrm{chla-mea}}\right] / \left[X^i{}_{\mathrm{chla-est}}+Y^i{}_{\mathrm{chla-mea}}\right] * 200\% \tag{17}$$

where the subscript i represents an individual data point, and n is the number of samples. When used to evaluate the accuracy of the CHLA model, $X_{\mathrm{chla\text{-}est}}$ and $Y_{\mathrm{chla\text{-}mea}}$ are the estimated and measured values of CHLA, respectively.

IV. Results and Analysis

A. Error Analysis of Retrieved CHLA

First, GOCI L1B data with the same date follow the field sampling data were selected and processed by GDPS1.4.1, GDPS2.0, Seadas_Default, and Seadas_MUMM atmospheric correction algorithms, respectively, and four groups of R_{rs} data were obtained. Then, OC2, YOC, OC3G, and OC2M-HI retrieval algorithms were used to retrieve the CHLA concentration of each group of R_{rs} data, and 16 sets of calculation results were obtained by combining four atmospheric correction algorithms with four CHLA concentration retrieval algorithms. According to the principle of spatial–temporal matching (the spatial range no more than 300 m and the time range no more than ±5 h), the retrieved CHLA concentration data were paired with the in situ CHLA concentration data for comparative analysis. The specific results were shown in Fig. 2, and different colors of the dots represent different atmospheric correction algorithms we used:

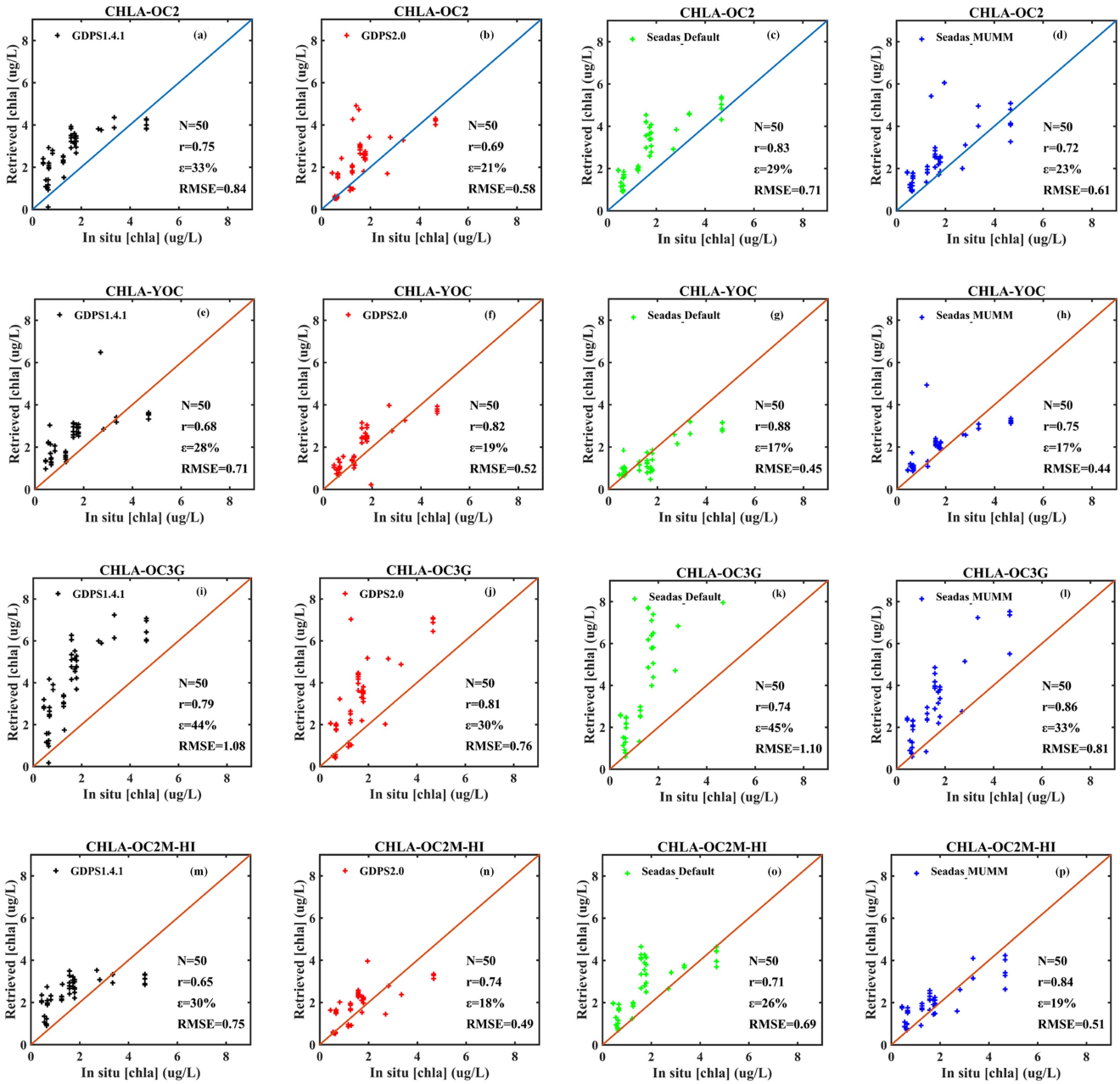

Fig. 2. Comparison figures of 16 sets of retrieved CHLA concentration data from GOCI with in-situ data. (a)–(d) Comparison result between retrieved CHLA data by using OC2 algorithm under four atmospheric correction algorithms and in situ CHLA data. (e)–(h) Comparison result between retrieved CHLA data by using YOC algorithm under four atmospheric correction algorithms and in situ CHLA data. (i)–(l) Comparison result between retrieved CHLA data by using OC3G algorithm under four atmospheric correction algorithms and in situ CHLA data. (m)–(p) Comparison result between retrieved CHLA data by using OC2M-HI algorithm under four atmospheric correction algorithms and in situ CHLA data.

black dots represent GDPS1.4.1, red dots represent GDPS2.0, green dots represent Seadas_Default, and blue dots represent Seadas_MUMM.

It can be concluded that when the CHLA concentration retrieval algorithm is OC2, the accuracy of CHLA concentration retrieved from GOCI by using GDPS2.0 atmospheric correction algorithm performs slightly better than the other three atmospheric correction algorithms. The correlation coefficient between retrieved CHLA concentration data from this combined and the in situ CHLA concentration data is 0.69, with an average relative error of 21% and a root mean square error of 0.58 [see Fig. 2(a)–(d)]. When the CHLA concentration retrieval algorithm is YOC, the performance of the Seadas_Default atmospheric correction algorithm and the Seadas_MUMM atmospheric correction algorithm is comparable, both of which are superior to the other two atmospheric correction algorithms [see Fig. 2(e)–(h)]. When the CHLA concentration retrieval algorithm is OC3G, the comparison results between the CHLA concentration data obtained from the four atmospheric correction algorithms and the measured data are generally similar,

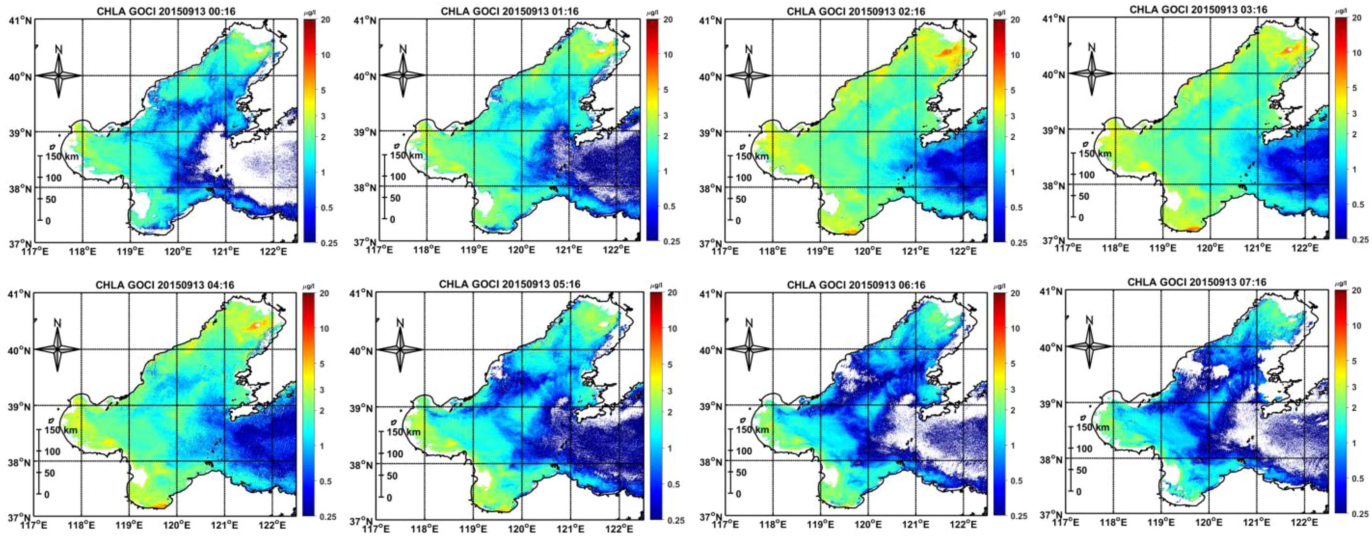

Fig. 3. Eight spatial distribution figures of CHLA concentration monitored by GOCI on 13 September, 2015.

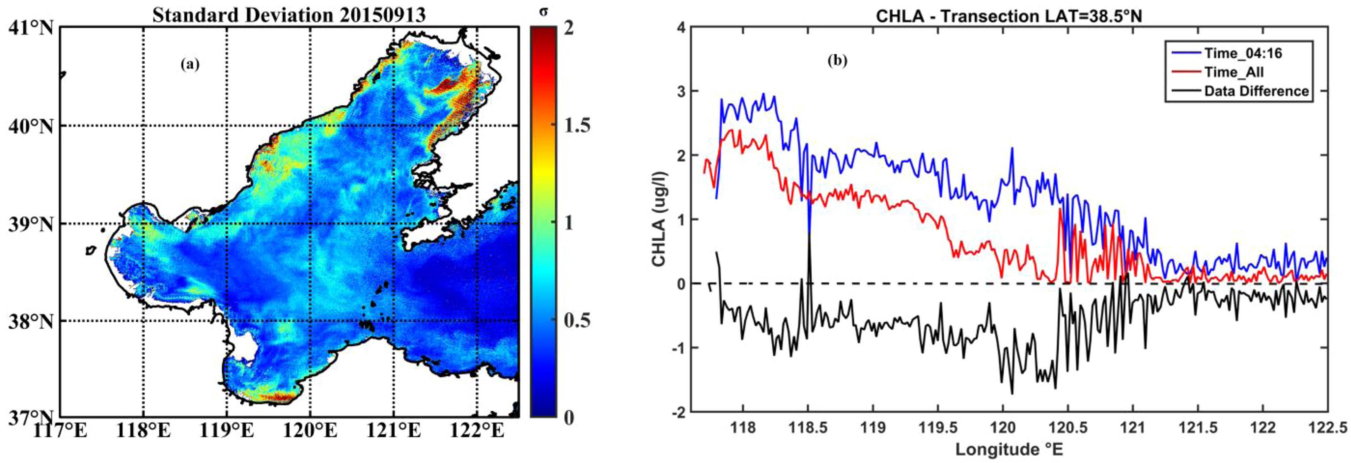

Fig. 4. (a) Standard deviation distribution of eight-scene CHLA concentration data in one day of 13 September, 2015. (b) Comparison of CHLA concentration changes along 38.5°N cross section, the blue line is the CHLA concentration value retrieved from the GOCI single-scene imaging data (04:16 UTC), the red line is the mean value of CHLA concentration retrieved by GOCI imaging data from eight-scene throughout the day, and the black line is the difference results of the two. Data difference = CHLA_Time_all - CHLA_Time_04.

all significantly higher than the measured CHLA concentration data. This OC3G algorithm has poor adaptability in the Bohai Sea, and the model coefficients need to be optimized and adjusted [see Fig. 2(i)–(l)]. For the OC2M-HI algorithm, the comparison results between the CHLA concentration data obtained from the GDPS2.0 atmospheric correction algorithm or the Seadas_MUMM atmospheric correction algorithm and the in situ CHLA concentration data are generally similar, and both are superior to the other two atmospheric correction algorithms [see Fig. 2(m)–(p)].

It can be seen that for the same CHLA concentration retrieval model, there are significant differences in the CHLA concentration values caused by different atmospheric correction algorithms. The differences between the retrieval results obtained by different CHLA concentration retrieval models under the same atmospheric correction algorithm also cannot be ignored. In the Bohai Sea area, when applying GOCI data to monitor CHLA concentrations, it is necessary to simultaneously consider the combined results of atmospheric correction algorithms and CHLA concentration models. The results of this study show that the performance relationships of each combination are as follows: Seadas_Default_YOC ≈ Seadas_MUMM_YOC > GDPS2.0_OC2M-HI ≈ GDPS2.0_YOC ≈ Sedas_MUMM_OC2M-HI > Other combinations. Considering the doubts raised by some research results regarding the adaptability of NASA's standard atmospheric correction algorithm to case II coastal water bodies [62], [63], this article used the Seadas_MUMM atmospheric correction algorithm to process GOCI data in the subsequent analysis of CHLA concentration, and the retrieval model for CHLA concentration used YOC.

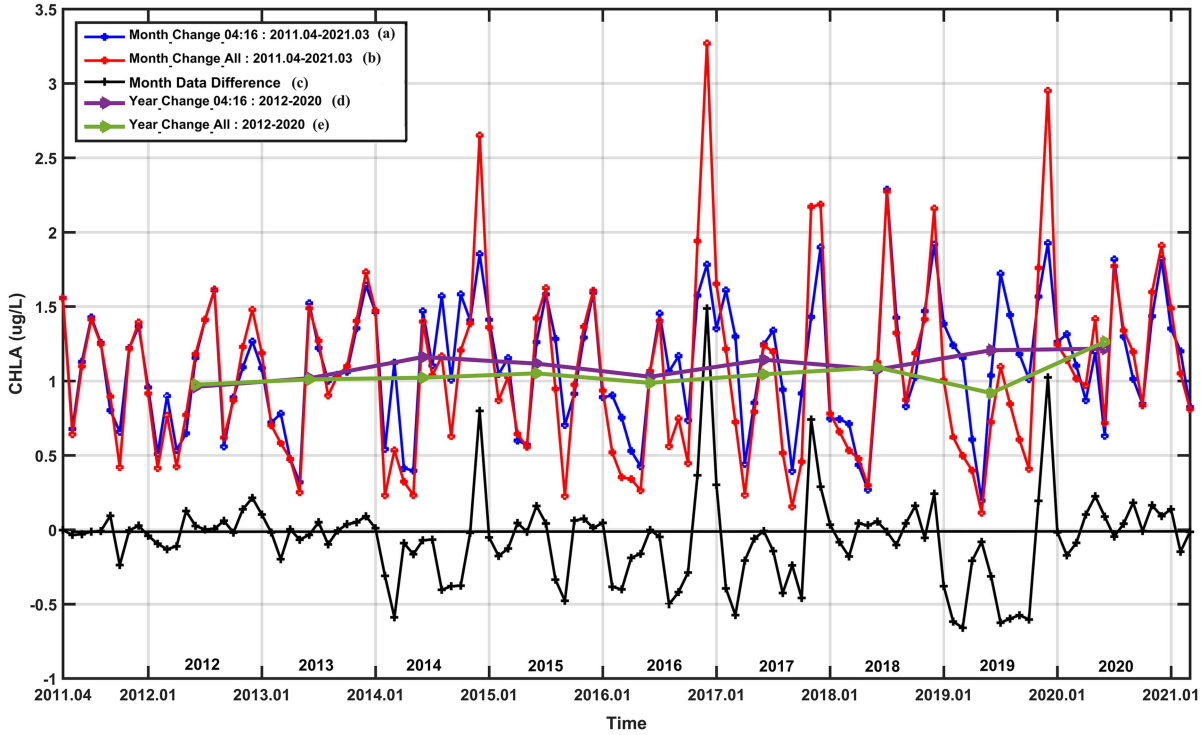

Fig. 5. Monthly and yearly average data of CHLA concentration in Bohai Sea monitored by GOCI: (a) blue line: monthly mean CHLA concentration obtained based on the daily single-scene GOCI imaging data (04:16 UTC), (b) red line: monthly mean CHLA concentration obtained based on the daily eight-scene GOCI imaging data, (c) black line: the difference between the above two (month data difference = Month_CHLA_Time_all - Month_CHLA_Time_04), (d) purple line: annual mean CHLA concentration obtained based on the daily single-scene GOCI imaging data (04:16 UTC), and (e) green line: annual mean CHLA concentration obtained based on the daily eight-scene GOCI imaging data.

B. GOCI Monitoring Results of CHLA

GOCI is the first geostationary ocean color satellite sensor of the world. Compared with the conventional polar-orbiting satellite sensors, such as Terra/MODIS and Aqua/MODIS, GOCI can acquire eight scene observations per day (see Fig. 3), significantly improving the coverage of daily observations. This study quantitatively and analytically investigates the spatial distribution and temporal variation patterns of CHLA concentration in the Bohai Sea using high-frequency GOCI data compared with traditional low-sampling-frequency polar-orbiting satellite sensors at daily, monthly, and yearly scales. It is worth noting that considering 04:16 (UTC) time is close to the transit time of most traditional polar-orbiting water-color satellite sensors, the imaging data of GOCI 04:16 (UTC) time are selected in this study to approximate the results of traditional polar-orbiting ocean color satellite sensors (denoted as CHLA_Time_04), and compare it with the average value of the eight GOCI observations (denoted as CHLA_Time_all) to analyze the differences between the two.

Fig. 3 shows the spatial distribution of CHLA concentration monitored by eight scenes of hourly imaging data in Bohai Sea on 13 September, 2015. It is obvious that the concentration of CHLA in Bohai Sea is significantly higher from 02:16 to 04:16 than at other times. Especially in the central Bohai Sea, the hourly variation characteristics of CHLA concentration were significant. Fig. 4(a) shows the standard deviation distribution of eight-scene CHLA concentration data in the day of 13 September, 2015. In the whole Bohai Sea area except the Bohai Strait, the standard deviation of the CHLA value observed in eight scenes during the day is about 0.5 μg/L, and it can even reach 1.0 μg/l or more in the coastal waters. Fig. 4(b) shows the comparison of CHLA concentration retrieval results between GOCI single-scene observation data (UTC 04:16) and averaged eight-scene observation data on 13 September, 2015 according the cross section at 38.5°N. We found that the difference between the two can be up to $\sim$2 μg/l [see Fig. 4(b)]. Those results indicate that the daily CHLA concentration monitoring results obtained from the frequency of single-scene per day cannot effectively characterize the daily average CHLA concentration in a specific region. Then, whether the results of analyzing the long-term spatio–temporal variation of CHLA concentration by using single-scene data per day or eight-scene data per day will also be different? In this study, we compared the results of CHLA concentration in the total Bohai Sea (37°–41°N and 117°–122°E) between the two observation frequencies on the monthly and yearly scales, and a detailed quantitative analysis of the differences was performed (see Fig. 5). The results show that the monthly average CHLA concentration based on the daily single-scene data from GOCI over the past decade (blue line in Fig. 5) differs significantly in some months from the monthly average CHLA concentration obtained from the daily eight-scene imaging data from GOCI (red line in Fig. 5), with the difference values ranging from -0.66 μg/l to 1.49 μg/l (black line in Fig. 5). The largest difference in CHLA concentration between the two

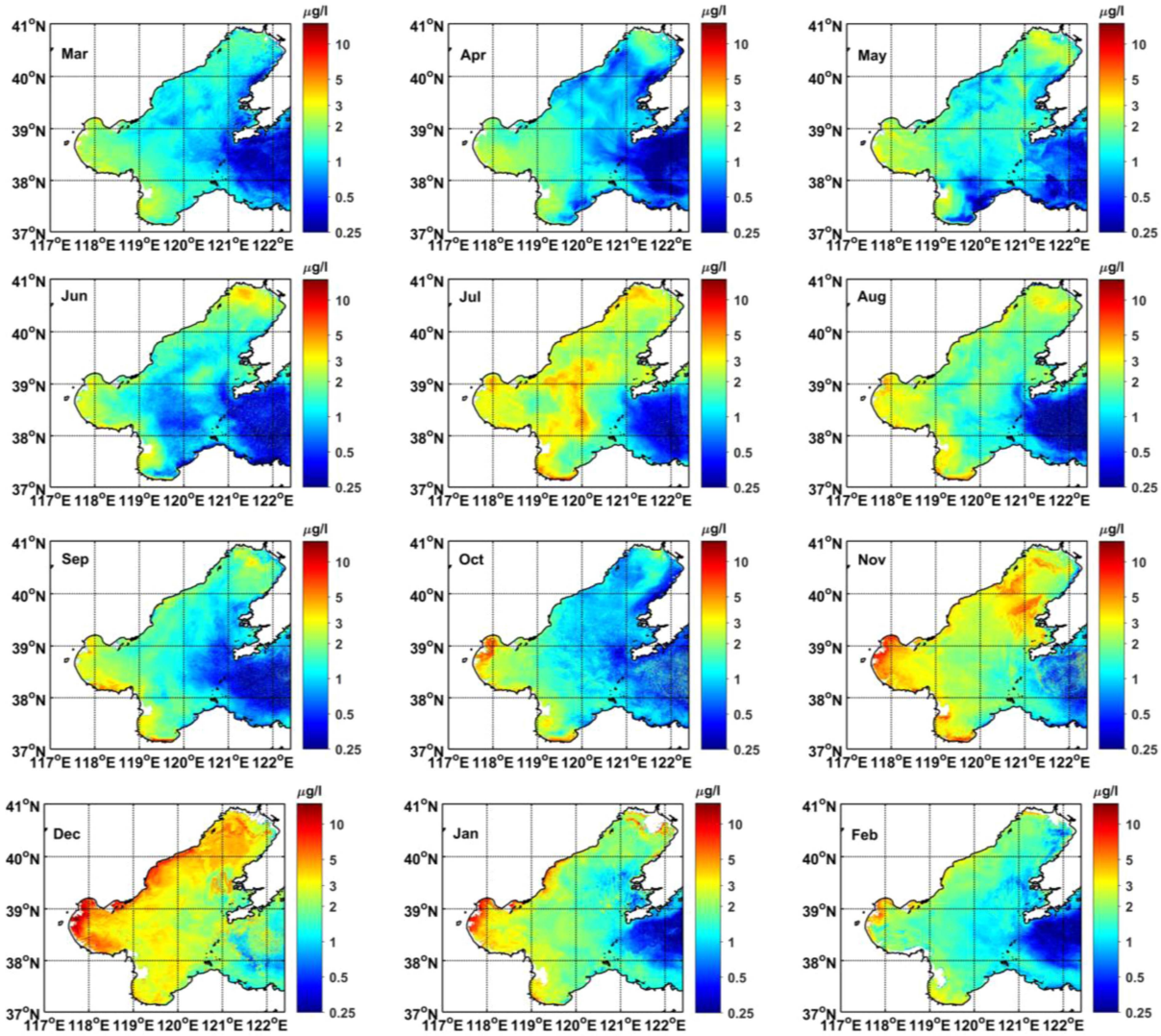

Fig. 6. Monthly average data results of GOCI monitoring of CHLA concentration in Bohai Sea from April 2011 to March 2020 over the decade. Each line from top to bottom represents the four seasons of spring, summer, autumn, and winter.

occurred in December 2016, reaching 1.49 μg/l, followed by December 2019 and then December 2014. The annual difference between 2012 and 2020 in CHLA concentration based on the two is faint and much less than the monthly average (purple and green lines in Fig. 5). Although the yearly change trends of CHLA concentration over the decade are generally consistent based on the two data (single-scene versus eight-scene daily average observations), the CHLA concentration values vary from each other, and even the results of short-term changes are inconsistent. For example, there is a decreasing trend from 2014 to 2017, and an increasing trend from 2019 to 2020 based on GOCI daily single-scene imaging data (purple line in Fig. 5), which is consistent with previously published trends by using MODIS. However, the annual variation trend of CHLA concentration based on GOCI daily eight-scene imaging data shows a more gradual change from 2014 to 2017 (green line in Fig. 5). Actually this difference is understandable, because the single-scene GOCI data are acquired at 04:16 (UTC), according to the results of CHLA daily variation (see Fig. 3), this is the moment when CHLA concentration is higher, and the average value of GOCI 8 data from morning to night will effectively change the mean result of selecting only higher CHLA concentration value, which is caused by the different data sources we use. The subsequent analysis of the spatial–temporal variation process of CHLA concentration in the Bohai Sea will use data obtained from GOCI's daily eight-scene imaging data.

C. Spatial and Temporal Distribution of CHLA in Bohai Sea

In this article, CHLA concentration data in Bohai Sea were retrieved based on the GOCI data from April 2011 to March 2020, and the monthly mean spatial distribution results for the decade were obtained (see Fig. 6). Each line from top to bottom in Fig. 6 represents the four seasons of spring (March, April, May), summer (June, July, August), autumn (September, October, November), and winter (December, January, February). We can find that the CHLA concentration in spring and autumn was lower than that in summer and winter. The high CHLA in

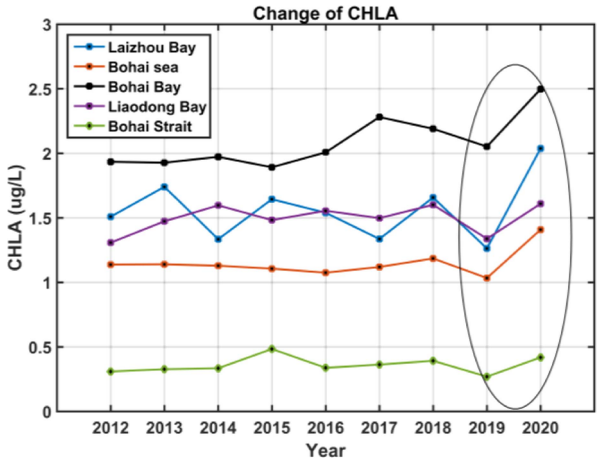

Fig. 7. Results of interannual variation of CHLA concentration in different regions of the Bohai Sea during 2012–2020.

summer can be explained that higher sea surface temperatures encourage the growth of phytoplankton. The high CHLA in winter can be explained that strong winter winds and lower sea surface temperature enhance vertical mixing and nutrients from subsurface layers brought to the euphotic layer. The results also show that the CHLA concentration value increases gradually from deep water to shallow water, with a general distribution trend of high near shore and low far shore. The concentration of CHLA in the Bohai Strait is the lowest, and the concentration of CHLA in the central of the Bohai Sea area is lower than that in the other three bays.

To better analyze the spatial–temporal variations, this study provides annual average concentration change lines for the Central Bohai Sea, three bay areas, and the Bohai Strait from 2012 to 2020 (see Fig. 7). It was observed that the annual average concentration of CHLA in the Bohai Bay region (black line in Fig. 7) was significantly higher than in other areas of the Bohai Sea, whereas the concentration in the Bohai Strait (green line in Fig. 7) was significantly lower than in other Bohai Sea regions. During the period from 2012 to 2020, the CHLA concentration in the Bohai Bay region exhibited a noticeable increasing trend, whereas the concentrations in Laizhou Bay and Liaodong Bay showed relatively small annual variations, maintaining an average around 1.5 μg/l. Except for the year 2020, the Central Bohai Sea region exhibited a relatively stable annual average CHLA concentration from 2012 to 2019, consistently around 1.15 μg/l. In the Bohai Strait, the annual average CHLA concentration remained below 0.5 μg/l. Furthermore, it is noteworthy that, except for the Bohai Strait in 2020, the CHLA concentrations in other Bohai Sea regions reached their highest levels in nearly a decade.

D. Change of CHLA in Bohai Sea During COVID-19 Lockdown

At the end of 2019, the COVID-19 broke out in China, which had varying degrees of impact on human activities both nationwide and globally for a long period of time thereafter. From 23 January to 8 April, 2020, Wuhan, Hubei Province, was under a "lockdown" period, and many other regions in China, including cities along the Bohai Sea, implemented numerous epidemic prevention policies. This pandemic had a significant impact on people's daily lives and also resulted in reduced coastal activities and a slowdown in the development of the marine fisheries economy, which in turn had a considerable impact on the marine ecosystem. In this study, we analyzed the changes in CHLA concentration in the Bohai Sea before and after the COVID-19 outbreak using monthly average data from 2015 to 2020 (Figs. 8 and 9). It is important to note that we are only presenting the change facts of CHLA concentration during the COVID-19 period, which does not necessarily imply that the variations of CHLA concentration during this time were caused by the lockdown due to COVID-19.

The results show that the CHLA concentration in Bohai Sea during the strictest period (February to April in 2020) of COVID-19 control measures in 2020 (black line in Fig. 8) was significantly higher than the same period of the previous year (2019, green line in Fig. 8), and also higher than the average level during the same period from 2015 to 2019 (red line in Fig. 8). With the end of the lockdown in Wuhan in April, the relaxation of the national epidemic prevention policy, the increase of industrial activities in cities around the Bohai Sea, and the orderly resumption of production and work, the CHLA concentration in Bohai Sea showed a rapid rising trend from April to May 2020, with an increase over 0.4 μg/l. In contrast to the upward trend in CHLA concentration during the same period from May to July in 2015–2019, the CHLA concentration in the Bohai Sea in May–July 2020 showed a different pattern, with a rapid decrease (decrease of over 0.7 μg/L) followed by a rapid increase (increase of over 1.0 μg/L). The chlorophyll a concentration in the Bohai Sea reached its lowest value in June 2020, deviating significantly from the previous months with the lowest CHLA concentration in the Bohai Sea (May or September). The anomaly change of monthly CHLA concentration shows a significant increasing trend from January to May in 2020 (see Fig. 9).

V. Discussion

A. Uncertainty in the Assessment of CHLA Retrieval Performance

Due to the limited amount of in situ measured CHLA concentration data, there are still some uncertainties and limitations in evaluating the results of this study. First, these uncertainties may arise from the less stringent spatio–temporal matching criteria between the satellite and in situ CHLA concentration data. Generally, a time window of $\pm$3 h should be set to obtain the matching pairs between the satellite data and the measured data [64]. However, in this study, we set the time window to $\pm$5 h in order to obtain a sufficient number of matching data. In future studies, more in situ CHLA data need to be further acquired, and the time matching window should be strictly controlled within $\pm$3 h. Second, the selection of atmospheric correction algorithms and CHLA concentration retrieval models was limited. In this study, only four atmospheric correction algorithms and four CHLA concentration retrieval models were used. In future

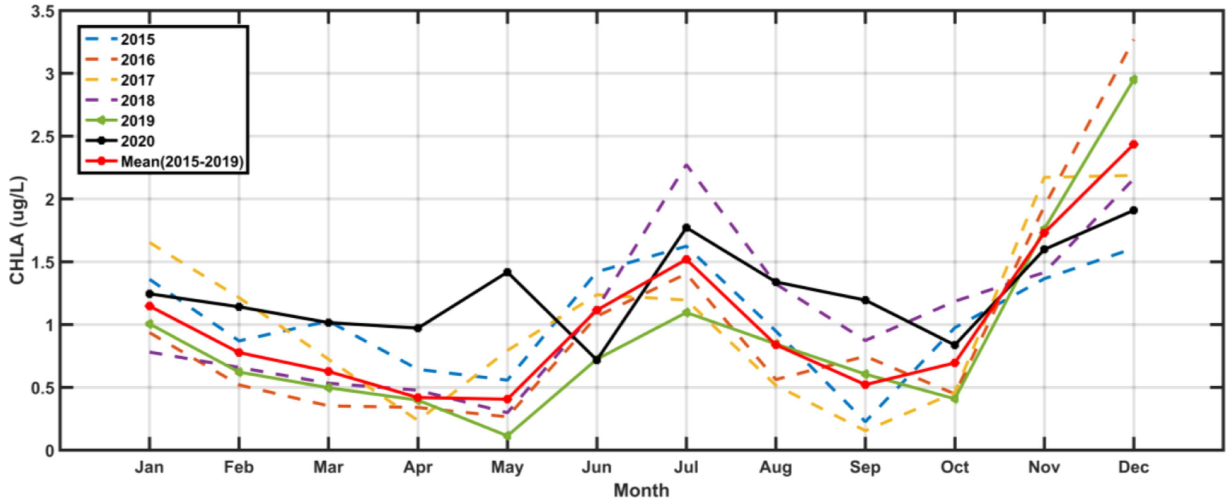

Fig. 8. Comparison diagram of monthly mean CHLA concentration changes in Bohai Sea from 2015 to 2020.

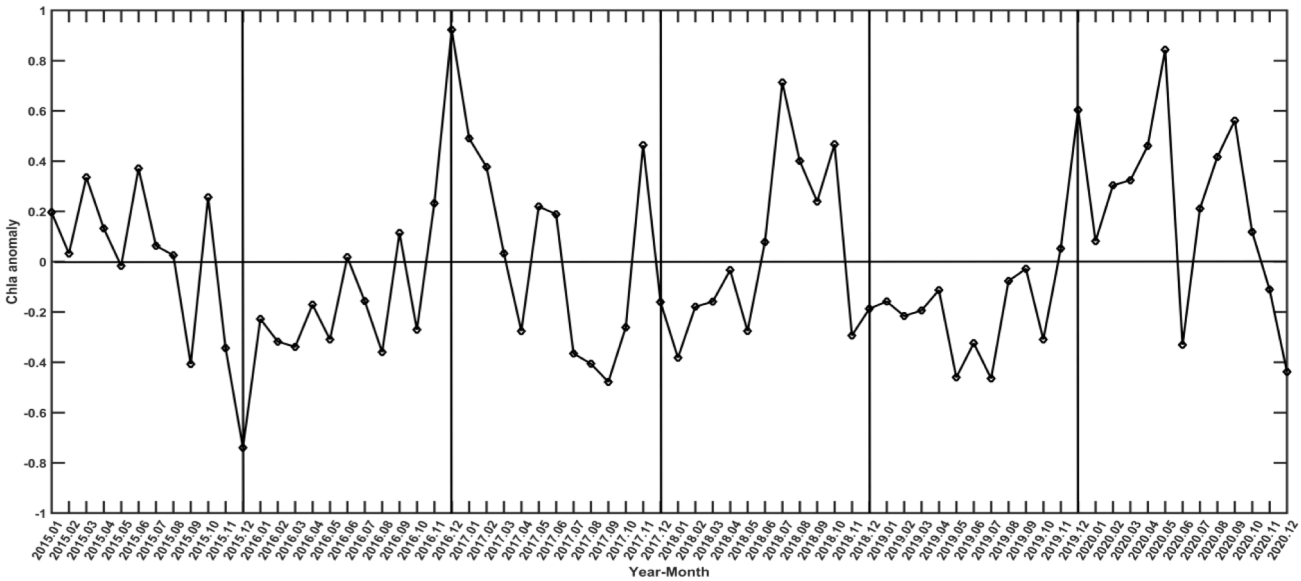

Fig. 9. Anomaly change of CHLA concentration in Bohai Sea from January 2015 to December 2020.

research, other atmospheric correction algorithms, such as those based on artificial neural network algorithms [65], and other CHLA concentration retrieval models, such as the generalized additive model proposed by the authors in [62] and [66], can be attempted to further improve the comparative results of this study.

B. Reliability of GOCI Data in Marine Ecological Monitoring

The GOCI satellite sensor data used in this article can provide eight-scene observation data from 8 A.M. to 15 P.M. of the Beijing local time every day. Compared with the traditional polar-orbiting satellite sensor, which can only provide single-scene observation data per day (such as MODIS), its data sampling frequency was increased by eight times, and the effective data coverage rate of daily average monitoring data was also significantly improved. GOCI has irreplaceable advantages in monitoring short-term and long-term changes of marine ecological parameters. The results of this article show that there are differences between the monitoring results of CHLA concentration based on eight-scene of GOCI data and that based on single view of GOCI data (equivalent to the traditional polar satellite sensor data) in the comparison of daily mean (see Fig. 4), monthly mean, and annual mean (see Fig. 5). Although many studies have also mentioned the advantages of GOCI monitoring marine ecological environment, most of them focus on the analysis of its hourly changes [42], [67], and there is no clear quantitative analysis of the differences between GOCI multiscene sampling data and single-scene sampling data as in this study. The results of this study indicate that early conclusions on the temporal–spatial changes of marine ecological parameters (such as CHLA concentration) based on traditional

low-sampling frequency polar-orbiting satellite data should be treated with caution [9], [68]. Although the high-frequency sampling frequency of GOCI has partially improved the effective coverage of daily monitoring data in the target sea area, the effective data coverage of GOCI satellite is still insufficient due to the influence of clouds, fog, solar flares, and thick aerosols, and these missing data will seriously affect the spatio–temporal continuity of water color remote sensing products. It even has a certain impact on the related research results of spatio–temporal changes. In the next research, it is still necessary to consider developing a data reconstruction algorithm that is suitable for GOCI high-frequency sampling characteristics to further perfect the research results of this article. In addition, some reports have raised doubts about the usability of dawn and dusk monitoring data obtained by GOCI sensors, although results of the study by Feng et al. [69] show that the quality of the GOCI dawn and dusk monitoring data is reliable at 412–680 nm. But the amount of in situ measured CHLA concentration data obtained in this study is limited. There are not sufficient conditions to evaluate the CHLA concentration products retrieved from the morning and evening monitoring data of GOCI. This remains one of the aspects that needs further improvement in subsequent research. One of the purposes of this article is to encourage research groups that own a lot of field data to supplement the analysis of this section.

C. CHLA in the Different Areas of Bohai Sea

From 2012 to 2020, the CHLA in the Bohai Strait were in a low state for a long time. The reason may be that the Bohai Strait is the channel connecting the Bohai Sea and the Yellow Sea, and a large amount of salt water in the Yellow Sea flows into it, so the water environment is very unfavorable for the growth of phytoplankton [44]. The Central Bohai Sea area is far from the land, and the impact of human activities in this area is lower than that in the three bays. Moreover, the high-concentration salt water exchanged from the Yellow Sea through the Bohai Strait also affects the stability of the environment in this area, which is not conducive to the aggregation of phytoplankton. Therefore, the concentration of CHLA in this area is higher than that in the Bohai Strait but lower than that in the Bohai Bay, Laizhou Bay, and Liaodong Bay. The Bohai Bay, Laizhou Bay, and Liaodong Bay are surrounded by the Bohai economic circle with a high degree of industrialization and a relatively dense population, and they are also the main receiving areas for a large number of rivers, such as the Yellow River flowing into Laizhou Bay, the Liaohe River flowing into Liaodong Bay, and the Luanhe River flowing into the northern area of Bohai Bay [70]. Extensive mariculture areas are situated on both sides of the estuary, and high CHLA concentration appears in the three bays due to the substantial nutrient discharge directly into the bays. In particular, Bohai Bay is the hub of shipping in North China. It is surrounded by land on three sides and adjacent to the land of Hebei, Tianjin, and Shandong. We suspect that the prosperous industrial production and other activities along the coast lead to a significant increase in the amount of nutrients discharged into Bohai Bay, which in turn promotes algae reproduction, resulting in a higher concentration of CHLA in the water body than in the other two bays [44]. So, a variety of reasons that lead to the spatio–temporal variability of CHLA in areas of the Bohai Sea are not completely consistent (Figs. 7 and 8).

TABLE II
CITIES AND START TIMES OF COVID-19 LOCKDOWN POLICIES IN BOHAI RIM

City	Start time
Qin huang dao	25.01.2022
Tang shan	28.01.2022
Dong ying	30.01.2022
Hu lu dao	05.02.2022
Jin zhou	05.02.2022
Pan Jin	05.02.2022
Da Lian	05.02.2022
Tian jin	06.02.2022
Cang zhou	09.02.2022

D. Uncertainty of Factors for Drastic Change of CHLA in Bohai Sea in 2020

The detailed changes of CHLA concentration in Bohai Sea before and after COVID-19 are given in Section IV-D of this article. Compared with the same period level in 2019 or the same period average in 2015–2019, the CHLA concentration in more than 92% of the whole sea areas was significantly increased in the period from January to May of 2020, when the epidemic prevention and control period was relatively strict (see Fig. 10). The lockdown and restriction measures implemented by coastal cities around the Bohai Sea during COVID-19 (see Table II) [71] have alleviated the pressure of human activities on marine ecology, which is one of the possible reasons for this change. However, previous studies have shown that CHLA concentration is not only affected by human activities, but also by natural factors, such as precipitation, wind speed, sea surface temperature, and nutrient salts [72]. Therefore, the cause of drastic changes in CHLA concentration in Bohai Sea in 2020 should be analyzed by combining the dual factors of natural environment and human activities to better quantify the proportion of each influencing factor. Here, we applied the GMI monthly average rain rate, sea surface temperature, and wind speed data from 2015 to 2020 to analyze the causes of the changes (see Fig. 11). We can find that the average rain rate in 2019 was about 0.15 mm/h, which is significantly lower than the 0.42 mm/h in 2018. The average wind speed in 2019 also decreased to 5.1 m/s from 5.3 m/s in 2018. The sea surface temperature in 2019 did not change significantly, only changing from 14.6 °C in 2018 to 14.9 °C. Therefore, the decrease of CHLA concentration in Bohai Sea in 2019 can be attributed to the decrease of runoff caused by the decrease of rainfall, thus reducing the input of terrestrial nutrients into the ocean. At the same time, the small decrease of wind speed more or less weakens the water mixing, which affects the vertical transport of nutrients from the depth of the water and inhibits the growth of phytoplankton. However, in 2020, the mean wind speed continued to decrease to 5.0 m/s, the mean rainfall was about 0.18 mm/h, and the mean sea surface temperature was about 15.0°, which were not much higher than that in 2019. If the impact of human activities was

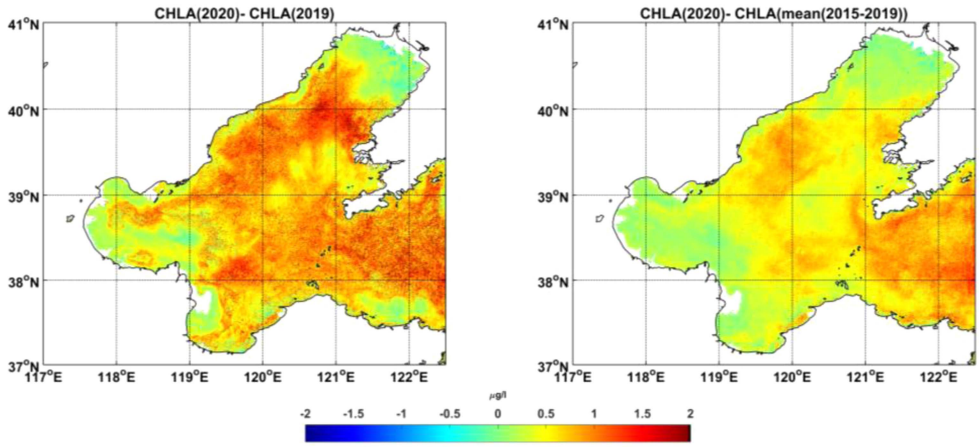

Fig. 10. Difference value of average CHLA concentration in Bohai Sea from January to May in 2020 compared with the same period in 2019 (left-hand side), and compared with the same period in 2015–2019 (right-hand side).

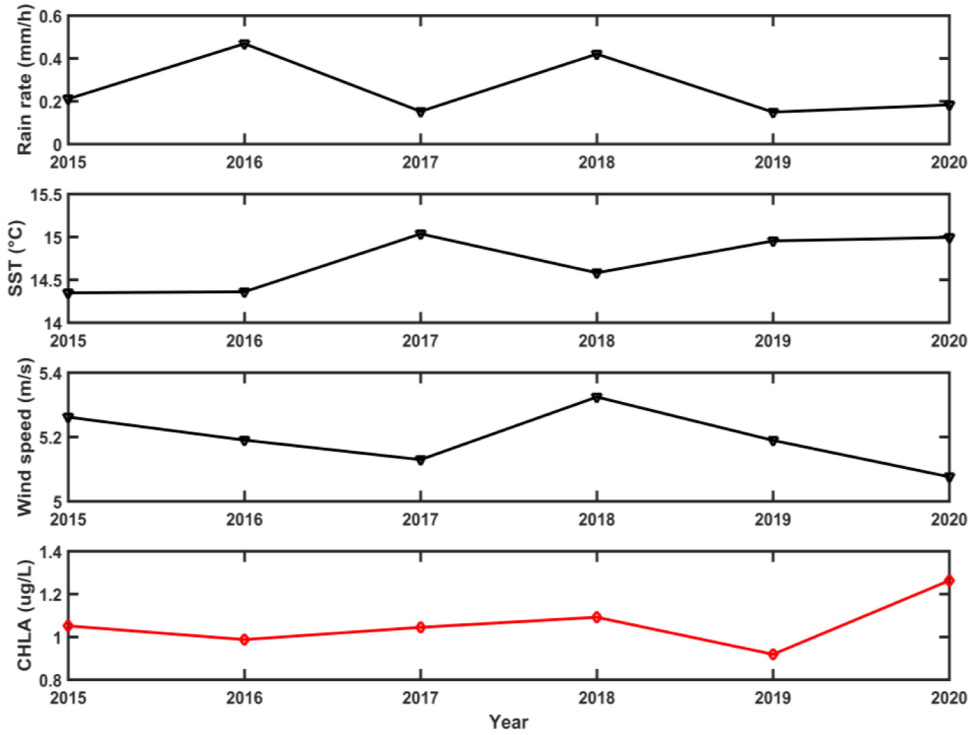

Fig. 11 Yearly changes of rain rate, sea surface temperature, wind speed, and CHLA concentration in Bohai Sea from 2015 to 2020.

not considered, convincing explanation should be that changes in these natural factors will not lead to drastic changes in the concentration of CHLA in the Bohai Sea in 2020. However, the results of this study show that the average concentration of CHLA in Bohai Sea in 2020 has reached the highest value in this decade. Therefore, we infer that the unusually high value of CHLA concentration in the Bohai Sea in 2020 has a high probability to be related to the abnormal human activities during COVID-19. However, it is worth noting that the resolution of GMI data is low, which may affect the certainty of the analysis results. The conclusions of this section of the study need to be supplemented with more data on other nutrients, such as nitrogen and phosphorus.

VI. Conclusion

The adaptability of four CHLA concentration retrieval models (OC2, YOC, OC3G, and OC2M-HI) under four atmospheric correction algorithms (GDPS1.4.1, GDPS2.0, Seadas Default, and Seadas MUMM) in the Bohai Sea was evaluated based on in situ CHLA concentration data. A clear quantitative analysis was conducted on the differences in the spatial–temporal distribution

of CHLA concentration in the Bohai Sea monitored by GOCI based on eight-scene sampling data and single-scene sampling data (which can be seen similar to the results of traditional polar-orbiting satellite data). The results of this study indicate that the differences in CHLA concentration values caused by different atmospheric correction algorithms cannot be ignored. It is not recommended to use OC2 and OC3G CHLA concentration retrieval models in the Bohai Sea. To obtain CHLA concentration data products with high retrieval accuracy, both atmospheric correction algorithms and CHLA concentration retrieval models need to be considered simultaneously, and the best combination of the two should be selected. The comparison with in situ CHLA data shows that the combination of atmospheric correction algorithms based on Seadas_Default or Seadas_MUMM and YOC CHLA concentration retrieval model is more suitable for GOCI data to retrieve CHLA concentration in the Bohai Sea. At the same time, the research results of this article also suggest that we should be cautious about the conclusions obtained from early research works on the spatial–temporal changes of marine ecological parameters (such as CHLA concentration) based on traditional polar-orbiting satellite data with low sampling frequency.

Acknowledgment

The authors would like to thank the KOSC for providing GOCI data and various versions of GDPS software, and also to NASA Ocean Biology Processing Group for providing SeaDAS software.

References

[1] X. Gao, F. Zhou, and C. T. Chen, "Pollution status of the Bohai Sea: An overview of the environmental quality assessment related trace metals," *Environ. Int.*, vol. 62, pp. 12–30, Jan. 2014, doi: 10.1016/j.envint.2013.09.019.

[2] S. Liu et al., "Water quality assessment by pollution-index method in the coastal waters of Hebei Province in western Bohai Sea, China," *Mar. Pollut. Bull.*, vol. 62, no. 10, pp. 2220–2229, Oct. 2011, doi: 10.1016/j.marpolbul.2011.06.021.

[3] X. Ning et al., "Long-term environmental changes and the responses of the ecosystems in the Bohai Sea during 1960–1996," *Deep Sea Res. Part II: Topical Stud. Oceanogr.*, vol. 57, no. 11-12, pp. 1079–1091, 2010, doi: 10.1016/j.dsr2.2010.02.010.

[4] Q. Tang, X. Jin, J. Wang, Z. Zhuang, Y. Cui, and T. Meng, "Decadal-scale variations of ecosystem productivity and control mechanisms in the Bohai Sea," *Fisheries Oceanogr.*, vol. 12, no. 4-5, pp. 223–233, 2003, doi: 10.1046/j.1365-2419.2003.00251.x.

[5] P. Kasprzak, J. Padisák, R. Koschel, L. Krienitz, and F. Gervais, "Chlorophyll a concentration across a trophic gradient of lakes: An estimator of phytoplankton biomass?," *Limnologica*, vol. 38, no. 3-4, pp. 327–338, 2008, doi: 10.1016/j.limno.2008.07.002.

[6] N. Ha, K. Koike, and M. Nhuan, "Improved accuracy of chlorophyll-a concentration estimates from MODIS imagery using a two-band ratio algorithm and geostatistics: As applied to the monitoring of eutrophication processes over Tien Yen Bay (Northern Vietnam)," *Remote Sens.*, vol. 6, no. 1, pp. 421–442, 2013, doi: 10.3390/rs6010421.

[7] B. Fründt, J. W. Dippner, and J. J. Waniek, "Chlorophyll a reconstruction from in situ measurements: 1. Method description," *J. Geophys. Res. Biogeosciences*, vol. 120, no. 2, pp. 237–245, 2015, doi: 10.1002/2014JG002691.

[8] V. V. Povazhnyi, "Determination of the chlorophyll 'a' concentration using a combined method based on measurements with a modified photometer," *Oceanology*, vol. 52, pp. 561–565, 2012, doi: 10.1134/s0001437012040078.

[9] M. Xu et al., "A 21-year time series of global leaf chlorophyll content maps from MODIS imagery," *IEEE Trans. Geosci. Remote Sens.*, vol. 60, Sep. 2022, Art. no. 4413513, doi: 10.1109/TGRS.2022.3204185.

[10] M. Darecki, S. Kaczmarek, and J. Olszewski, "SeaWiFS ocean colour chlorophyll algorithms for the southern Baltic Sea," *Int. J. Remote Sens.*, vol. 26, no. 2, pp. 247–260, 2007, doi: 10.1080/01431160410001720298.

[11] L. Sun, M. Guo, and X. Wang, "Ocean color products retrieval and validation around China coast with MODIS," *Acta Oceanologica Sinica*, vol. 29, no. 4, pp. 21–27, 2010, doi: 10.1007/s13131-010-0047-6.

[12] W. J. Moses et al., "Estimation of chlorophyll-a concentration in turbid productive waters using airborne hyperspectral data," *Water Res.*, vol. 46, no. 4, pp. 993–1004, Mar. 2012, doi: 10.1016/j.watres.2011.11.068.

[13] H. Li et al., "Assessment of satellite retrieval algorithms for chlorophyll-a concentration under high solar zenith angle," in *Proc. SPIE 9999, Remote Sens. Ocean, Sea Ice, Coastal Waters, Large Water Regions*, Edinburgh, U.K., Oct. 19, 2016, doi: 10.1117/12.2240164.

[14] M. R. Al Shehhi, I. Gherboudj, J. Zhao, and H. Ghedira, "Improved atmospheric correction and chlorophyll-a remote sensing models for turbid waters in a dusty environment," *ISPRS J. Photogrammetry Remote Sens.*, vol. 133, pp. 46–60, 2017, doi: 10.1016/j.isprsjprs.2017.09.011.

[15] E. S. Pereira and C. A. E. Garcia, "Evaluation of satellite-derived MODIS chlorophyll algorithms in the northern Antarctic Peninsula," *Deep Sea Res. Part II: Topical Stud. Oceanogr.*, vol. 149, pp. 124–137, 2018, doi: 10.1016/j.dsr2.2017.12.018.

[16] G. H. Tilstone et al., "Performance of ocean colour chlorophyll a algorithms for Sentinel-3 OLCI, MODIS-Aqua and Suomi-VIIRS in open-ocean waters of the Atlantic," *Remote Sens. Environ.*, vol. 260, 2021, Art. no. 112444, doi: 10.1016/j.rse.2021.112444.

[17] G. Dall'Olmo, A. A. Gitelson, and D. C. Rundquist, "Towards a unified approach for remote estimation of chlorophyll-a in both terrestrial vegetation and turbid productive waters," *Geophys. Res. Lett.*, vol. 30, no. 18, pp. 1–4, 2003, doi: 10.1029/2003GL018065.

[18] W. J. Moses, A. A. Gitelson, S. Berdnikov, and V. Povazhnyy, "Satellite estimation of chlorophyll-a concentration using the red and NIR bands of MERIS—The Azov Sea case study," *IEEE Geosci. Remote Sens.*, vol. 6, no. 4, pp. 845–849, Oct. 2009, doi: 10.1109/lgrs.2009.2026657.

[19] C. Hu, Z. Lee, and B. Franz, "Chlorophyll a algorithms for oligotrophic oceans: A novel approach based on three-band reflectance difference," *J. Geophys. Res-Oceans*, vol. 117, no. C1, 2012, Art. no. C01011, doi: 10.1029/2011JC007395.

[20] S. Mishra and D. R. Mishra, "Normalized difference chlorophyll index: A novel model for remote estimation of chlorophyll-a concentration in turbid productive waters," *Remote Sens. Environ.*, vol. 117, pp. 394–406, 2012, doi: 10.1016/j.rse.2011.10.016.

[21] W. Yang, B. Matsushita, J. Chen, T. Fukushima, and R. Ma, "An enhanced three-band index for estimating chlorophyll-a in turbid case-II waters: Case studies of Lake Kasumigaura, Japan, and Lake Dianchi, China," *IEEE Geosci. Remote Sens. Lett.*, vol. 7, no. 4, pp. 655–659, Oct. 2010, doi: 10.1109/LGRS.2010.2044364.

[22] J. Gower, "Observations of in situ fluorescence of chlorophyll-a in Saanich Inlet," *Boundary-Layer Meteorol.*, vol. 18, no. 3, pp. 235–245, 1980, doi: 10.1007/BF00122022.

[23] K. A. Ali and W. J. Moses, "Application of a PLS-augmented ANN model for retrieving chlorophyll-a from hyperspectral data in case 2 waters of the Western Basin of Lake Erie," *Remote Sens.*, vol. 14, no. 15, pp. 3729–3746, 2022, doi: 10.3390/rs14153729.

[24] J. Luo et al., "Research progress in the retrieval algorithms for chlorophyll-a, a key element of water quality monitoring by remote sensing," *Remote Sens. Technol. Application*, vol. 36, no. 3, pp. 473–488, 2021, doi: 10.11873/j.issn.1004-0323.2021.3.0473.

[25] X. Li, J. Sha, and Z.-L. Wang, "Application of feature selection and regression models for chlorophyll-a prediction in a shallow lake," *Environ. Sci. Pollut. Res.*, vol. 25, pp. 19488–19498, 2018, doi: 10.1007/s11356-018-2147-3.

[26] S. B. Hooker and C. R. McClain, "The calibration and validation of SeaWIFS data," *Prog. Oceanogr.*, vol. 45, no. 3, pp. 427–465, 2000, doi: 10.1016/s0079-6611(00)00012-4.

[27] S. Guo et al., "MODIS ocean color product downscaling via spatio-temporal fusion and regression: The case of chlorophyll-a in coastal waters," *Int. J. Appl. Earth Observation Geoinf.*, vol. 73, pp. 340–361, 2018, doi: 10.1016/j.jag.2018.06.004.

[28] E. Siswanto et al., "Empirical ocean-color algorithms to retrieve chlorophyll-a, total suspended matter, and colored dissolved organic matter absorption coefficient in the Yellow and East China Seas," *J. Oceanogr.*, vol. 67, no. 5, pp. 627–650, 2011, doi: 10.1007/s10872-011-0062-z.

[29] G. Dall'Olmo, A. A. Gitelson, D. C. Rundquist, B. Leavitt, T. Barrow, and J. C. Holz, "Assessing the potential of SeaWiFS and MODIS for estimating chlorophyll concentration in turbid productive waters using red and near-infrared bands," *Remote Sens. Environ.*, vol. 96, no. 2, pp. 176–187, 2005, doi: 10.1016/j.rse.2005.02.007.

[30] Z. Lee, K. L. Carder, and R. A. Arnone, "Deriving inherent optical properties from water color: A multi-band quasi-analytical algorithm for optically deep waters," *Appl. Opt.*, vol. 41, no. 27, pp. 5755–5772, 2002, doi: 10.1364/AO.41.005755.

[31] J. Wei and Z. P. Lee, "Retrieval of phytoplankton and color detrital matter absorption coefficients with remote sensing reflectance in an ultraviolet band," *Appl. Opt.*, vol. 54, no. 4, pp. 636–649, 2015, doi: 10.1364/ao.54.000636.

[32] X. He, Y. Bai, D. Pan, J. Tang, and D. Wang, "Atmospheric correction of satellite ocean color imagery using the ultraviolet wavelength for highly turbid waters," *Opt. Exp.*, vol. 20, no. 18, pp. 20754–20770, 2012, doi: 10.1364/OE.20.020754.

[33] M. Wang and W. Shi, "Remote sensing of the ocean contributions from ultraviolet to near-infrared using the shortwaveinfrared bands: Simulations," *Appl. Opt.*, vol. 46, no. 9, pp. 1535–1547, 2007, doi: 10.1364/AO.46.001535.

[34] G. F. Moore, J. Aiken, and S. J. Lavender, "The atmospheric correction of water colour and the quantitative retrieval of suspended particulate matter in case II waters: Application to MERIS," *Int. J. Remote Sens.*, vol. 20, no. 9, pp. 1713–1733, 1999, doi: 10.1080/014311699212434.

[35] J.-H. Ahn, Y.-J. Park, J.-H. Ryu, B. Lee, and I. S. Oh, "Development of atmospheric correction algorithm for Geostationary Ocean Color Imager (GOCI)," *Ocean. Sci. J.*, vol. 47, no. 3, pp. 247–259, 2012, doi: 10.1007/s12601-012-0026-2.

[36] C. Jamet, S. Thiria, and C. Moulin, "Use of a neurovariational inversion for retrieving oceanic and atmospheric constituents from ocean color imagery: A feasibility study," *J. Atmospheric Ocean. Technol.*, vol. 22, pp. 460–475, 2005, doi: 10.1175/JTECH1688.1.

[37] T. Schroeder, I. Behnert, M. Schaale, J. Fischer, and R. Doerffer, "Atmospheric correction algorithm for MERIS above case-2 waters," *J. Remote Sens.*, vol. 28, pp. 1469–1486, 2007, doi: 10.1080/01431160600962574.

[38] J. Brajard, R. Santer, M. Crpon, and S. Thiria, "Atmospheric correction of MERIS data for case-2 waters using a neuro-variational inversion," *Remote Sens. Environ.*, vol. 126, pp. 51–61, 2012, doi: 10.1016/j.rse.2012.07.004.

[39] J. Brajard, C. Jamet, S. Thiria, C. Moulin, and M. Crepon, "Use of a neuro-variational inversion for retrieving oceanic and atmospheric constituents from satellite ocean color sensor: Application to absorbing aerosols," *Neural Netw.*, vol. 22, pp. 460–475, 2006, doi: 10.1016/j.neunet.2006.01.015.

[40] C. P. Kuchinke, H. R. Gordon, L. W. Harding, and K. J. Voss, "Spectral optimization for constituent retrieval in Case II waters II: Validation study in the Chesapeake Bay," *Remote Sens. Environ.*, vol. 113, pp. 610–621, 2009, doi: 10.1016/j.rse.2008.11.002.

[41] R. Chomko, H. Gordon, S. Maritorena, and D. Siegel, "Simultaneous retrieval of oceanic and atmospheric parameters for ocean color imagery by spectral optimization: A validation," *Remote Sens. Environ.*, vol. 84, no. 2, pp. 208–220, 2003, doi: 10.1016/S0034-4257(02)00108-6.

[42] X. Liu, Q. Yang, Y. Wang, and Y. Zhang, "Evaluation of GOCI remote sensing reflectance spectral quality based on a quality assurance score system in the Bohai Sea," *Remote Sens.*, vol. 14, no. 5, 2022, Art. no. 1075, doi: 10.3390/rs14051075.

[43] F. Zhai, W. Wu, Y. Gu, P. Li, X. Song, and P. Liu, "Interannual-decadal variation in satellite-derived surface chlorophyll-a concentration in the Bohai Sea over the past 16 years," *J. Mar. Syst.*, vol. 215, 2021, Art. no. 103496, doi: 10.1016/j.jmarsys.2020.103496.

[44] Y. Du, X. Zhang, S. Ma, and N. Yao, "Chlorophyll-a concentration variations in Bohai Sea: Impacts of environmental complexity and human activities based on remote sensing technologies," *Big Data Res.*, vol. 36, 2024, Art. no. 100440, doi: 10.1016/j.bdr.2024.100440.

[45] X.-Y. Liu et al., "Comparative study on transparency retrieved from GOCI under four different atmospheric correction algorithms in Jiaozhou Bay and Qingdao coastal area," *IEEE J. Sel. Topics Appl. Earth Observ. Remote Sens.*, vol. 17, pp. 2077–2089, Dec. 2023, doi: 10.1109/JSTARS.2023.3343572.

[46] R. Liu, J. Zhang, H. Yao, T. Cui, N. Wang, and Y. Zhang, "Hourly changes in sea surface salinity in coastal waters recorded by Geostationary Ocean Color Imager," *Estuarine, Coastal Shelf Sci.*, vol. 196, pp. 227–236, 2017, doi: 10.1016/j.ecss.2017.07.004.

[47] L. Sun, J. Jiang, and W. Zhu, "Remote sensing inversion and daily variation of CDOM based on GOCI in the Changjiang Estuary and adjacent waters," *Haiyang Xuebao*, vol. 39, no. 9, pp. 133–145, 2017, doi: 10.3969/j.issn.0253-4193.2017.09.013.

[48] J. Wang, J. Tang, W. Wang, Y. Wang, and Z. Wang, "Quantitative retrieval of chlorophyll-a concentrations in the Bohai–Yellow sea using GOCI surface reflectance products," *Remote Sens.*, vol. 15, 2023, Art. no. 5285, doi: 10.3390/rs15225285.

[49] Y. Qian et al., "Evaluation of ocean color products from Korean geostationary ocean color imager (GOCI) in Jiaozhou Bay and Qingdao coastal area," in *Proc. SPIE 9216, Int. Soc. Opt. Eng.*, Beijing, China, Dec. 18, 2014, doi: 10.1117/12.2069114.

[50] W. M. Kim, Y.-J. Park, and J. Ishizaka, "Evalution of chlorophyll retrievals from geostationary ocean color imager (GOCI) for the North-East Asian region," *Remote Sens. Environ.*, vol. 184, pp. 482–495, 2016, doi: 10.1016/j.rse.2016.07.031.

[51] J.-H. Ahn, Y.-J. Park, and H. Fukushima, "Comparison of aerosol reflectance correction schemes using two near-infrared wavelengths for ocean color data processing," *Remote Sens.*, vol. 10, 2018, Art. no. 1791, doi: 10.3390/rs10111791.

[52] J.-H. Ryu, H.-J. Han, S. Cho, Y.-J. Park, and Y.-H. Ahn, "Overview of geostationary ocean color imager (GOCI) and GOCI data processing system (GDPS)," *Ocean Sci. J.*, vol. 47, no. 3, pp. 223–233, 2012, doi: 10.1007/s12601-012-0024-4.

[53] J. H. Ahn, Y. J. Park, W. Kim, and B. Lee, "Vicarious calibration of the geostationary ocean color imager," *Opt. Exp.*, vol. 23, no. 18, pp. 23236–23258, 2015, doi: 10.1364/OE.23.023236.

[54] J.-H. Ahn, Y.-J. Park, W. Kim, and B. Lee, "Simple aerosol correction technique based on the spectral relationships of the aerosol multiple-scattering reflectances for atmospheric correction over the oceans," *Opt. Exp.*, vol. 24, no. 26, pp. 29659–29669, Dec. 2016, doi: 10.1364/OE.24.029659.

[55] H. R. Gordon and M. Wang, "Retrieval of water leaving radiance and aerosol optical thickness over the oceans with SeaWiFS: A preliminary algorithm," *Appl. Opt.*, vol. 33, no. 3, pp. 443–452, 1994, doi: 10.1364/AO.33.000443.

[56] R. P. Stumpf, R. A. Arnone, R. W. Gould, P. M. Martinolich, and V. Ransibrahmanakul, "A partially coupled ocean-atmosphere model for retrieval of water-leaving radiance from SeaWiFS in coastal waters," *NASA Tech. Memo.*, vol. 22, pp. 51–59, 2003.

[57] S. W. Bailey, B. A. Franz, and P. J. Werdell, "Estimation of near-infraredwater-leaving reflectance for satellite ocean color data processing," *Opt. Exp.*, vol. 18, no. 7, pp. 7521–7527, 2010, doi: 10.1364/OE.18.007521.

[58] Z. Ahmad et al., "New aerosol models for the retrieval of aerosol optical thickness and normalized water-leaving radiances from the SeaWiFS and MODIS sensors over coastal regions and open oceans," *Appl. Opt.*, vol. 49, pp. 5545–5560, 2010, doi: 10.1364/ao.49.005545.

[59] K. G. Ruddick, F. Ovidio, and M. Rijkeboer, "Atmospheric correction of SeaWiFS imagery for turbid coastal and inland waters," *Appl. Opt.*, vol. 39, no. 6, pp. 897–912, 2000, doi: 10.1364/AO.39.000897.

[60] S. Tassan, "Local algorithms using SeaWiFS data for the retrieval of phytoplankton, pigments, suspended sediment, and yellow substance in coastal waters," *Appl. Opt.*, vol. 33, pp. 2369–2378, 1994.

[61] J. E. O'Reilly, S. Maritorena, B. G. Mitchell, and D. A. Siegel, "Ocean color chlorophyll algorithms for SEAWIFS," *J. Geophysical Res.: Oceans*, vol. 103, no. C11, pp. 24937–24953, 1998, doi: 10.1029/98JC02160.

[62] M. Wang, J. Tang, and W. Shi, "MODIS-derived ocean color products along the China east coastal region," *Geophys. Res. Lett.*, vol. 34, no. 6, 2007, Art. no. L06611, doi: 10.1029/2006gl028599.

[63] D. A. Siegel et al., "Regional to global assessments of phytoplankton dynamics from the SeaWiFS mission," *Remote Sens. Environ.*, vol. 135, pp. 77–91, 2013, doi: 10.1016/j.rse.2013.03.025.

[64] S. W. Bailey and P. J. Werdell, "A multi-sensor approach for the on-orbit validation of ocean color satellite data products," *Remote Sens. Environ.*, vol. 102, no. 1-2, pp. 12–23, 2006, doi: 10.1016/j.rse.2006.01.015.

[65] C. Goyens, C. Jamet, and T. Schroeder, "Evaluation of four atmospheric correction algorithms for MODIS-aqua images over contrasted coastal waters," *Remote Sens. Environ.*, vol. 131, pp. 63–75, 2013, doi: 10.1016/j.rse.2012.12.006.

[66] Y. Wang, D. Liu, Y. Wang, Z. Gao, and J. K. Keesing, "Evaluation of standard and regional satellite chlorophyll-a algorithms for moderate-resolution imaging spectroradiometer (MODIS) in the Bohai and Yellow Seas, China: A comparison of chlorophyll-a magnitude and seasonality," *Int. J. Remote Sens.*, vol. 40, no. 13, pp. 4980–4995, 2019, doi: 10.1080/01431161.2019.1577579.

[67] Y. Zhou et al., "Monitoring multi-temporal and spatial variations of water transparency in the Jiaozhou Bay using GOCI data," *Mar. Pollut. Bull.*, vol. 180, Jul. 2022, Art. no. 113815, doi: 10.1016/j.marpolbul.2022.113815.

[68] K. K. Kivva and A. A. Kubryakov, "Seasonal and interannual variability of chlorophyll-a concentration in the Bering Sea found from satellite data," *Izvestiya, Atmospheric Ocean. Phys.*, vol. 57, no. 12, pp. 1643–1657, 2021, doi: 10.1134/S0001433821120136.

[69] Q. Feng, C. Jianyu, and X. Yuying, "Usability analysis GOCI twilight periods radiative transfer model data," *Mar. Inf.*, vol. 1, pp. 28–39, 2021, doi: 10.19661/j.cnki.mi.2021.01.005.

[70] S. Shang, Z. Lee, L. Shi, G. Lin, G. Wei, and X. Li, "Changes in water clarity of the Bohai Sea: Observations from MODIS," *Remote Sens. Environ.*, vol. 186, pp. 22–31, 2016, doi: 10.1016/j.rse.2016.08.020.

[71] X. Xiao, S. Huang, and J. He, "The impact of COVID-19 lockdown on the variation of sea surface chlorophyll-a in Bohai Sea, China," *Regional Stud. Mar. Sci.*, vol. 66, 2023, Art. no. 103163, doi: 10.1016/j.rsma.2023.103163.

[72] K. Zhang, X. Zhao, J. Xue, D. Mo, and D. Zhang, "The temporal and spatial variation of chlorophyll a concentration in the China Seas and its impact on marine fisheries," *Front. Mar. Sci.*, vol. 10, pp. 1–19, 2023, doi: 10.3389/fmars.2023.1212992.

Jing-wen Hu received the Ph.D. degree in marine information detection and processing from the Ocean University of China, Qingdao, China, in 2016.

She is currently an Associate Researcher with Shandong Marine Forecast and Hazard Mitigation Service, Qingdao. Her research interests include ocean remote sensing and marine disaster prevention.

Xiao-yan Liu received the M.S. degree in marine information detection and processing in 2014 from the Ocean University of China, Qingdao, China, where she is currently working toward the Ph.D. degree in three-dimensional observations of chlorophyll-a concentration around Shandong Peninsula.

Since 2014, she has been an Engineer with the Institute of Oceanographic Instrumentation, Qilu University of Technology (Shandong Academy of Sciences), Jinan, China. She is the author of more than 20 articles and holds two patents. Her research interests include ocean remote sensing and ocean optics.

Qi-xiang Wang received the Ph.D. degree in ecology from the Ocean University of China, Qingdao, China, in 2009.

He is currently a Researcher with Shandong Marine Forecast and Hazard Mitigation Service, Qingdao. His research interests include marine disaster prevention, ecological restoration, and ocean remote sensing.

Xin Li received the M.S. degree in engineering from Shandong University, Jinan, China, in 2011.

She is currently a Senior Engineer with Weifang Marine Development Research Institute, Weifang. Her research interests include marine observation and forecasting, marine environmental monitoring, and marine area management.

Wen-long Dong received the Ph.D. degree in ecology from the Ocean University of China, Qingdao, China, in 2016.

He is currently an Associate Researcher with Shandong Marine Forecast and Hazard Mitigation Service, Qingdao. His research interests include marine disaster prevention, ecological restoration, and ocean remote sensing.

Wei-qi Lin is currently working toward the bachelor's degree in marine technology (major) with the Qilu University of Technology (Shandong Academy of Sciences), Qingdao, China.

He is diligent, serious, and assiduous, and full of curiosity about related majors.

Jun-yue Zhang is currently working toward the bachelor's degree in marine technology (major) with the Qilu University of Technology (Shandong Academy of Sciences), Qingdao, China.

She is diligent and assiduous. Her research focuses on ocean remote sensing.

Ming-yu Li is currently working toward the bachelor's degree majoring in measurement and control technology and instruments (marine measurement and control direction) with the Qilu University of Technology (Shandong Academy of Sciences), Qingdao, China.

His research focuses on marine disaster prevention.

Zhi-hong Wu received the M.S. degree in biological engineering from the Ocean University of China, Qingdao, China, in 2016.

He is currently a Researcher with Shandong Marine Forecast and Hazard Mitigation Service, Qingdao. His research interests include coastal and marine ecosystem conservation and marine disaster prevention.